Experimental study of drag force on bridge-pier models with different geometries using a strain-gauge sensor

Mohammad Shirali [1], Mohammad Heidarnejad [*,1], Aslan Egdernezhad [1], Alireza Masjedi [1], Amin Bordbar [1]

1. Department of Water Science Engineering, Ahv.C., Islamic Azad University, Ahvaz, Iran.

***Corresponding Author:**
Mohammad Heidarnejad

Email: mo.heidar@iau.ac.ir
Received: 2026.07.28
Accepted: 2026.10.01
J. Hydraul. Struct., 2027;13(2):1-14
DOI: 10.22055/jhs.2026.52785.1392

ABSTRACT

One of the forces entering hydraulic structures is the drag force, which is usually obtained through empirical relationships. These relationships have been presented in many studies through simulation and wind tunnel testing. In this study, the drag force entering hydraulic structures was examined using strain gauge technology. Use of this method allows direct measurement of the force entering the structure. The experiments were undertaken under controlled laboratory flow conditions in a wide range of hydraulic parameters, with the drag force measured directly using a strain gauge-based device. The results indicated that the drag coefficient and force are heavily affected by the base geometry, surface roughness, and flow conditions. Also, the common empirical relations for calculating the drag force differed from reality by up to 780% in some conditions. It was also found that the geometric shape of the structure and its dimensions have a significant impact on the amount of drag force.

KEYWORDS
Drag Force, Hydraulic Structures, Strain Gauge, Bridge-Pier Models.

1. Introduction

One of the forces that flow imposes on structures is drag force. In physics and fluid dynamics, drag force refers to forces that act to resist the motion of an object within a fluid [1]. When an object moves in a fluid, an interaction takes place between the object and the fluid whereby corresponding forces are created [2]. Effective forces can include shear stress owing to viscosity as well as forces due to pressure. The outcome of these forces is referred to as drag force in the flow direction and lift force in the direction perpendicular to the flow direction [3]. Since it is difficult to calculate the stress and pressure distribution on the surface of an object accurately, experimental methods are usually employed to estimate drag force [4]. Experiments performed on small models in wind tunnels, water tunnels, or other inventive methods allow for generalization to real samples through dimensional analysis. One of the dimensionless quantities utilized in calculating drag force is the drag coefficient (Cd). Cd is a dimensionless quantity used in fluid dynamics to calculate the drag force on an object moving in a fluid [5]. This quantity is usually represented by different symbols such as Cd, Cx, and Cw (Cifuentes and Kim, 2017) [6].

Study of experimentally investigates the influence of discrete transverse roughness elements on flow resistance in a rectangular open-channel flume. Experiments were conducted with three longitudinal spacing ratios (S/K = 6, 12, and 24) under steady discharges of 15, 20, and 25 L s−1. The relationships between the Froude number (Fr) and both drag force (FD) as well as drag coefficient (CD) were analyzed. The results indicated that as Fr increased, so did the drag force in general in most configurations (particularly at larger spacing). However, the drag coefficient exhibited an overall descending trend with Fr in the majority of cases, consistent with the normalization by dynamic pressure [7]. Also, bed roughness strongly influenced flow resistance, turbulence structure, and energy dissipation [8]. The drag coefficient is a function of the Reynolds number as well as the relative surface roughness, and can be calculated from Table 1 [9].

Table 1: Drag coefficient

Row	Shape	Drag Coefficient
1	●	0.47
2	◀	0.5
3	■	1.05
4	◆	0.80
5	▬	0.82

Based on Table 1, the drag force can be calculated using Equation 1 [10].

$$F_{Df} = \frac{1}{2}\rho U^2 C_{Df} A \quad (1)$$

In Equation 1, U is the flow velocity, A represents the effective cross-sectional area, and ρ denotes the fluid density [11].

Recent studies have demonstrated that accurate estimation of the hydrodynamic forces acting on bridge piers and other hydraulic structures, particularly under flood-flow and open-channel conditions, remains an important issue in hydraulic engineering. Although many conventional relationships primarily consider the drag coefficient (C_d) as a function of the Reynolds number, recent studies have shown that this assumption may not be sufficient for free-surface flows and complex hydraulic conditions.

In the study, Do and Nguyen [12] conducted a numerical simulation using the SPH method to model the impact of water flow on the Canh Nang Bridge in Vietnam. They concluded that the SPH model allows for recording the dynamic flow responses between the bridge body and the tsunami wave, and using this method, they could calculate the water resistance coefficient (Cd). They also concluded that further research is necessary to explore the effect of structural parameters, such as the shape and size of the bridge superstructure, on its response to the flow shock during a flood.

Elsewhere, Cifuentes and Kim [6] calculated drag coefficients for fishing cages using the physical model method. They found that the drag coefficients from previous methods were only valid for low-strength cages exposed to flows of lower than 0.5 m / s. In a numerical study by Han et al. [13], the difference in drag coefficients of different bridge sections was examined using the pressure distribution method and 3D numerical simulations under various conditions. According to the results, as the section becomes simpler, the frictional drag can grow and its value approaches a maximum at an angle of contact close to zero degrees; also, its value drops with increasing the angle of contact.

Novak and Domínguez Alonso [14] investigated the flow around a cylindrical bridge pier in an open channel using three-dimensional Smoothed Particle Hydrodynamics (SPH) simulations and proposed a relationship between the drag coefficient and the Froude number. Their results indicated that, under the investigated conditions, using a constant drag coefficient, as adopted in some formulations such as Eurocode 1, does not necessarily

provide the most accurate estimation. This finding highlights the importance of experimentally investigating drag coefficients under actual water-flow conditions. Mostefaoui et al [15] experimentally investigated the drag force exerted by supercritical open-channel flows on emerging obstacles. They measured the force acting on rectangular obstacles over a range of Froude numbers and obstacle-width-to-flow-depth ratios. Their results showed that the drag coefficient increased with increasing obstacle-width-to-depth ratio and decreased with increasing Froude number. These findings demonstrate the importance of considering both obstacle geometry and flow conditions when determining drag force and are directly relevant to the present study, which experimentally examines the effects of pier geometry and flow conditions on drag force. Okamoto and Sanjou [16] investigated driftwood accumulation and jam formation around bridge piers and also measured the drag force acting on the pier and the corresponding changes in the drag coefficient. Their results indicated that changes in the geometric configuration around the pier can substantially modify the hydrodynamic force acting on the structure. The relevance of this study to the present research lies in demonstrating that the use of a constant drag coefficient without considering the actual geometric and hydraulic conditions may lead to inaccurate estimation of the actual drag force. Tang et al [17] investigated the drag and lift forces acting on bed sediments in open-channel flow under different Froude-number conditions. Their study demonstrated that changes in flow structure and Froude number can significantly modify the distribution of hydrodynamic forces. Although the primary focus of that study was sediment particles rather than bridge piers, its findings are relevant to experimental investigations of drag force because they emphasize the dependence of hydrodynamic forces on flow conditions.

In 2026, recent studies have increasingly focused on the effects of multiple-pier interactions and geometric configuration on hydrodynamic forces. A study on two cylindrical piers in open-channel flow investigated the effects of pier spacing and alignment angle on the hydrodynamic forces. The results showed that the upstream pier could produce a shielding effect and that the force acting on the downstream pier varied depending on the relative spacing and alignment angle. The study demonstrated that both geometry and structural arrangement play important roles in determining hydrodynamic forces [18]. Furthermore, Anzani et al [19] experimentally investigated the effects of transverse roughness elements and their spacing ratio on drag force and drag coefficient in an open channel. The experiments were conducted for three spacing ratios ((S/K=6), 12, and 24) and different flow discharges. Their results indicated that, in many configurations, drag force increased with increasing Froude number, whereas the drag coefficient generally exhibited a decreasing trend. The spacing between roughness elements also modified the wake structure and consequently affected the drag force. These findings demonstrate that geometry, flow conditions, and the characteristics of the surrounding flow field should be considered simultaneously when analyzing drag force. Liang et al. (2026) investigated the effect of flow deflection angle on hydraulic forces associated with bridge-pier protection structures using RANS-based numerical modeling. Their results further emphasized the importance of structural geometry and its interaction with the approaching flow in controlling hydrodynamic forces.

Recent investigations of scale effects and downstream wake characteristics have also highlighted the importance of three-dimensional flow structures and hydrodynamic similarity. A 2025 study examining turbulent wake characteristics downstream of isolated bridge piers under laboratory and field conditions demonstrated that the wake region, vortex structures, and turbulence scales downstream of a pier exhibit complex

characteristics. Therefore, careful consideration of the flow field is necessary when attempting to extend laboratory-scale findings to real-world conditions. A review of recent studies published in 2025 and 2026 indicates that current research has mainly developed along three major directions: three-dimensional numerical modeling, investigation of the effects of the Froude number and hydraulic conditions, and evaluation of the influence of structural geometry and arrangement on hydrodynamic forces. Nevertheless, there remains a significant research gap in the direct experimental measurement of drag force under controlled water-flow conditions using an instrumented load-cell/strain-gauge system and the direct comparison of experimentally measured drag force with conventional empirical relationships.

2. Materials and Methods

In this research, the aim is to inspect the drag force on bridge piers as well as obstacles in the flow path. Obtaining accurate results and exploring the effect of effective parameters on drag force require construction of a drag force measuring device. For this purpose, a drag force measuring device was first designed and constructed using strain gauge technology. Then, using laboratory equipment, the drag force was measured and the accuracy of the relationships utilized to calculate it was ascertained.

2.1. Dimensional Analysis

To achieve the research objectives, first the parameters governing the hydraulics of the flow passing around the bridge piers are introduced Next, the effective parameters of this research are presented as dimensionless relations. The effective geometric, kinematic, and dynamic variables are reported in Table 2.
In Equation 2, the important parameters affecting the drag force are specified.

$$F_D = f(V, D, F_d, \rho, \nu, b, h, S_h, g) = 0 \quad (2)$$

By performing dimensional analysis, dimensionless numbers were obtained according to Equation 3.

$$F_D = \left(\frac{VD}{\upsilon}.\frac{V}{(gD)^{½,}}, \frac{\rho V^2 h}{\sigma}, \frac{h}{b}, \frac{D}{b}, S_h, \right) = 0 \quad (3)$$

In Equation 3, the well-known dimensionless parameters are the Reynolds number ($Re = \frac{VD}{\upsilon}$), Weber number (We=$\frac{\rho V^2 h}{\sigma}$), and Froude number ($Fr = \frac{V}{(gD)^{½,}}$). Since the We number is for linear flow and the Re number is applied for flow in pipelines, these two numbers were omitted. In order to calculate the Manning coefficient, the Strickler equation, which is Equation 4, is used.

$$n = \frac{d_{50}{}^{\frac{1}{6}}}{31.3} 0.032 d_{50}{}^{\frac{1}{6}} \quad (4)$$

In Equation 4, d_{50} represents the median particle diameter in feet (ft). The exact determination of this coefficient on the surfaces of commercially manufactured materials is challenging [20]. Thus, in this study, the surface of the measuring device was covered with coatings with different roughnesses to measure the impact of this parameter on the drag force.

Table 2: Effective parameters

Row	Parameter symbol	Parameter name	Description
1	V	Flow velocity	Variable
2	D	Bridge base diameter	Variable
3	g	Gravitational acceleration	9.8m/S^2
4	ρ	Unit mass of water	988/2Kg/m^3
5	Y	Kinematic viscosity	
6	b	Flume width	Constant
7	F_d	Drag force	
8	h	Water height	
9	S_h	Bridge base shape	Variable

2.2. Required tools and equipment:

The aim of this research is to accurately investigate drag force using an instrumented measurement system under water-flow conditions. To achieve this objective, a set of experimental equipment was required, as .described below

- Drag force measuring device (Dragmeter) .Instrumentationfor measuring the force exerted on the bridge structure
- Laboratory flume: Laboratory flume for simulating water flow
- Model of the foundations under study:Bridge-pier models for investigating the effects of geometry and dimensions on the applied force

2.3. Laboratory flume

The experiments in this study are undertaken in a flume whose walls are made of plexiglass and it is possible to observe the flow inside the flume (Figure 1).

In this study, the flow velocity and the velocity upstream of the device were measured using a point speedometer (upstream of the dragmeter). The dragmeter (Figure 1) was installed at the center of the flume, and the flow completely submerged the aluminum housing.

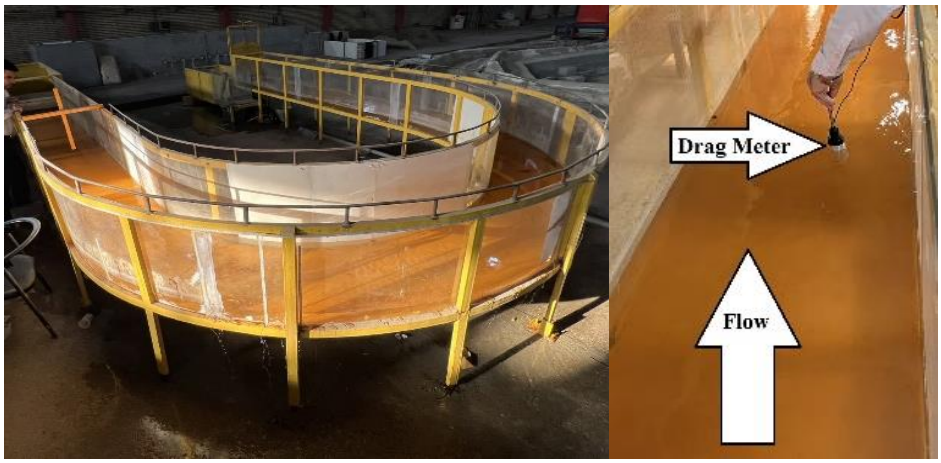


Figure 1: Cross-section of the laboratory flume and the location of the applied force measurement

3. Dragmeter

In this study, strain gauge technology was utilized to measure the drag force on water structures. The operating principles of the device were based on the fact that using an internal strain gauge, the drag force was converted into a corresponding signal with the data collected at a sampling rate of about 200 samples per second. Next, after processing, the output was provided to the researcher in the form of an Excel file at a rate of 23 samples per second (Figure 2). The measurement method in this design was carried out using a strain gauge sensor; so that the quantity applied to the structure created strain with the strain measured by the strain gauge. A strain gauge is a device for measuring strain. Strain is defined as the change in length relative to the initial length (i.e., the relative change in length). The applications of a strain gauge are numerous, with stress measurement being of its important applications. Stress is the force applied per unit area of a sample. Many load cells are made based on strain gauges. A similar structure is also used in some pressure gauges. In these sensors, the quantity to be measured (such as force in a load cell or pressure in a pressure gauge) causes a strain in a part of the sensor; the strain is then measured by the strain gauge (Figure 2).

To create the drag meter, the sensor cover was first designed, and then once the cover was made, the central core of the strain gauge was embedded inside it. In the next step, the electronic circuit was designed and built. The data collected from the sensor were directed to the circuit via four insulated wires. After initial processing by the relevant circuit, the data were transferred to the computer via an industrial RS485 transmitter and monitored by LabVIEW software (Figure 3).



Figure 2. View of the drag meter device

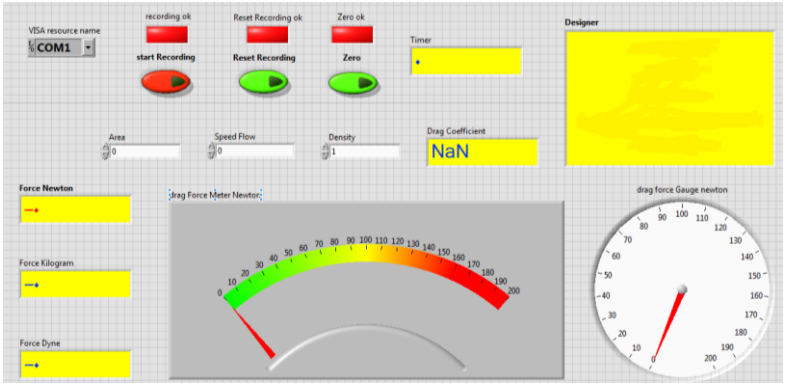


Figure 3. Software designed by Labview

In this research, a load cell sensor (strain gauge technology) was utilized to measure the drag force. All sensors needed to be calibrated after use and examined in the laboratory. Also, great care needed to be taken in selecting the sensor and its operation since each sensor was made for a specific environment and conditions, so selecting the sensor based on environmental conditions would require high accuracy.The device measures the pressure drag force exerted on a fully submerged bridge-pier model. This force acts normal to the pier model and in the flow direction; vortex-related effects and surface-friction forces are not directly measured by the device.

4. Research variables

This study explores the effect of geometric shape and roughness on the drag force on bridge piers. Accordingly, the designed experiments include the effective variables according to Table 3. Figure 4 displays the bridge pier model.

In Figure 4, three shapes of circles, triangles, and squares were made using cement to be mounted on the dragmeter device to enhance the accuracy and correspondence of the geometric shape to reality. Furthermore, to minimize the effects of the channel sidewalls, the ratio of the channel width to the pier diameter should be greater than 2.56. In the present experiments, the cylinder diameter was 15 cm and the channel width was 60 cm. Thus, the channel-width-to-pier-diameter ratio was calculated as follows, frac W/D=60/15= 4, where (W) is the channel width and (D) is the pier diameter. Therefore, the obtained ratio of 4 satisfies the recommended criterion for minimizing sidewall effects [21].

Table 3. Research variables

Variables	Model number	Variable mods
Cylindrical shape	3	Circle, square and triangle 10 to 50 liters
Flow rate (Q)	5	
Base dimensions (L)	3	
Total tests	45	



Figure 4. Three bridge foundation models

Before the tests, the strain gauge-based drag force measurement system was calibrated using known loads to establish the relationship between the strain output and the applied force. For repeatability, each test was repeated at least three times under the same flow conditions to ensure the repeatability of the measurements (The results were compared to ensure that the differences between the measurements remained minimal. In cases where a significant discrepancy was observed, the experiment was repeated. In addition, the mean value of the three experimental runs was calculated.). Further, the measurement uncertainty was estimated by considering the sensor accuracy (93%), load calibration error, and test repeatability, with the tests performed under steady flow conditions at controlled flow rates. Finally, the Froude number was calculated for each test case.

For each experiment, the sensor installation position and submergence depth were kept constant. First, the sensor was installed, after which the flow discharge was adjusted. Once the flow had stabilized, the force was recorded continuously for one minute. This procedure was repeated for all three bridge pier models at all flow discharge rates. The flowchart illustrating the research procedure is presented in Figure 5.

5. Results and Discussion

In this study, the drag force applied to circular (S), triangular (T) and square (C) structures was measured using a precision dragmeter. Thereafter, the results examined the effect of drag force on three geometric shapes while also comparing the force measured by the dragmeter with the force calculated from Equation 1 and Table 1. The dragmeter device collects a piece of data (the amount of applied force) every half second in each experiment, so in each simulation, the device outputs a total of 120 numbers (the applied force) in the form of a txt file An example of this output for a square with sides of 10 cm is outlined in Table 4.

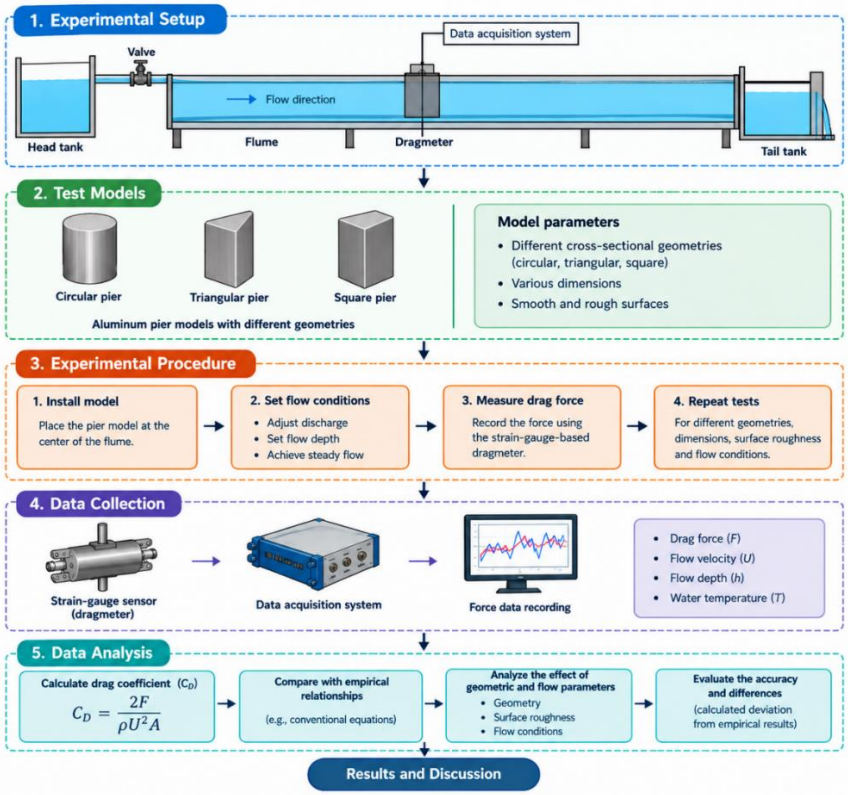


Figure 5. Flowchart of the Research Methodology

Table 4. Raw data for the T=10Cm model

Time	Force	Time	Force	Time	Force	Time	Force	Time	Force	Time	Force	Time	Force
0.5	0.079399	9.5	1.081412	18.5	0.034189	27.5	0.138624	36.5	0.315911	45.5	0.289070	54.5	0.339258
1	0.079473	10	0.186403	19	0.708404	28	0.138624	37	0.322319	46	0.307476	55	0.461313
1.5	0.079095	10.5	0.726722	19.5	1.692577	28.5	0.138624	37.5	0.343491	46.5	0.365279	55.5	0.539351
2	0.077935	11	0.726722	20	0.073377	29	0.304078	38	0.339160	47	0.315452	56	0.518828
2.5	0.077518	11.5	0.726722	20.5	0.075551	29.5	0.074594	38.5	0.241594	47.5	0.320158	56.5	0.403427
3	0.077326	12	0.726722	21	0.069431	30	0.069877	39	0.352775	48	0.315212	57	0.421239
3.5	0.077347	12.5	0.726722	21.5	0.212975	30.5	0.094881	39.5	0.258883	48.5	0.366384	57.5	0.398154
4	0.077191	13	0.091425	22	0.212975	31	0.320196	40	0.267524	49	0.306494	58	0.372206
4.5	0.077149	13.5	0.092799	22.5	0.212975	31.5	0.320196	40.5	0.171394	49.5	0.394729	58.5	0.375256
5	0.077382	14	0.092799	23	0.116119	32	0.320196	41	0.272125	50	0.283657	59	0.355332
5.5	0.077424	14.5	0.021704	23.5	0.116119	32.5	0.017650	41.5	0.285841	50.5	0.258929	59.5	0.133424
6	0.077505	15	0.021704	24	0.012042	33	0.017650	42	0.232358	51	0.208335	60	0.165895
6.5	0.231329	15.5	0.302024	24.5	0.012042	33.5	0.054705	42.5	0.222598	51.5	0.196693		
7	0.231329	16	0.109737	25	0.032830	34	0.012960	43	0.232174	52	0.211418		
7.5	0.231329	16.5	0.587326	25.5	0.060474	34.5	0.287046	43.5	0.181224	52.5	0.213573		
8	0.231329	17	2.963636	26	0.071113	35	0.153480	44	0.221747	53	0.182886		
8.5	0.231329	17.5	0.037135	26.5	0.243788	35.5	0.307356	44.5	0.206987	53.5	0.195243		
9	0.177961	18	0.037688	27	0.138624	36	0.322967	45	0.184511	54	0.004303		

As observed in Table 4, the accuracy of the device is up to 0.000001 Newton.Some values were also similar, indicating good repeatability of the flow conditions. In other words, the experimental conditions tended to reach a stable state; however, inherent hydraulic fluctuations prevented the flow from remaining perfectly constant.

To better understand the performance of the device, Figure 6 depicts graphs of the force applied to the structure over a period of 60 seconds.

As is clear from Figure 6, the applied force has a constant trajectory on average, but at times the force grows suddenly and applies a high force to the structure abruptly, which is very dangerous owing to its suddenness. The reason for these instantaneous changes in force is the flow of water, which at sometimes augments the applied force due to hydraulic conditions such as a whirlpool.

Next, we will explore the effect of the Froude number (Between 0.5 and 1.8) on the amount of force applied to the structure. In this section, the horizontal axes represent the Froude number and the vertical axes reflect the amount of force applied (Newtons (N)). The results of this section are presented in the graphs of Figures 7 to 9. The numbers 5, 7.5 and 10 also indicate the diameter (in a circular structure) as well as the dimensions of the sides (in a square and triangular structure) in centimeters.

According to Figure 7, with a 50% increase in the structure dimensions, the drag force rises by about 75%. Also, the difference between the measured force and the force calculated from Equation 1 is positive in all cases and under some conditions, it reaches up to 370%.

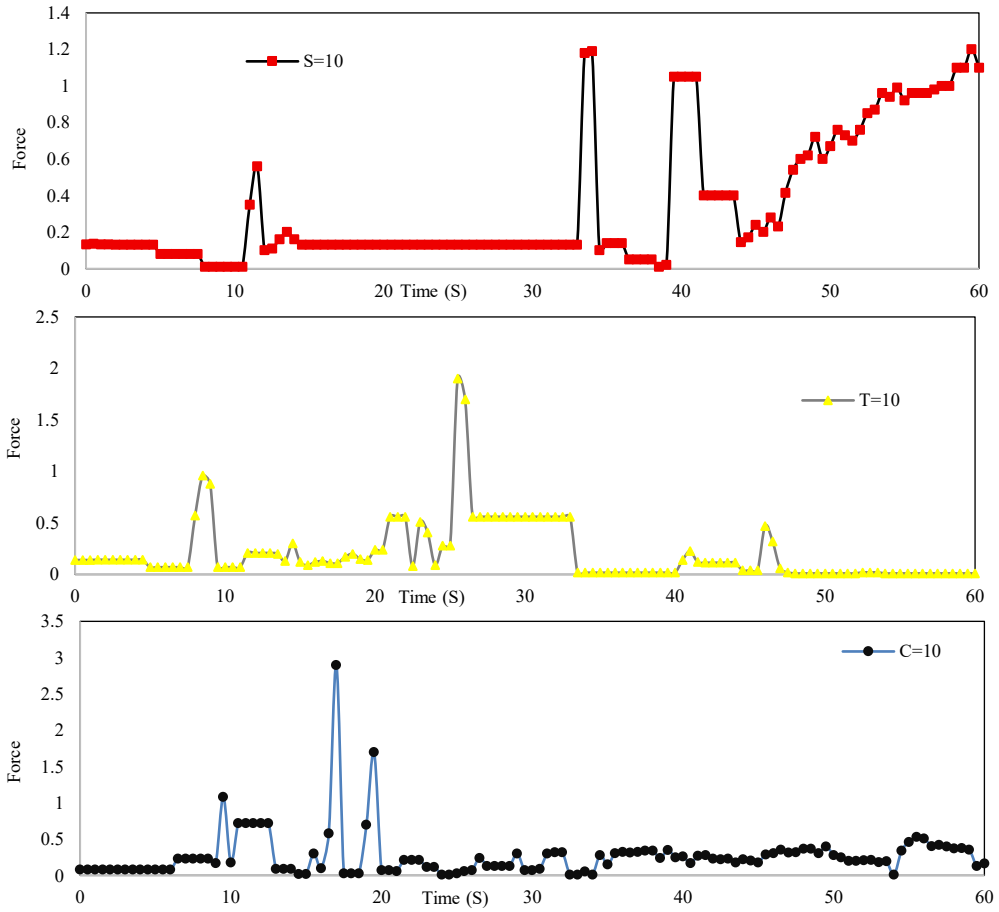


Figure 6. Force versus time graphs in 10 cm size

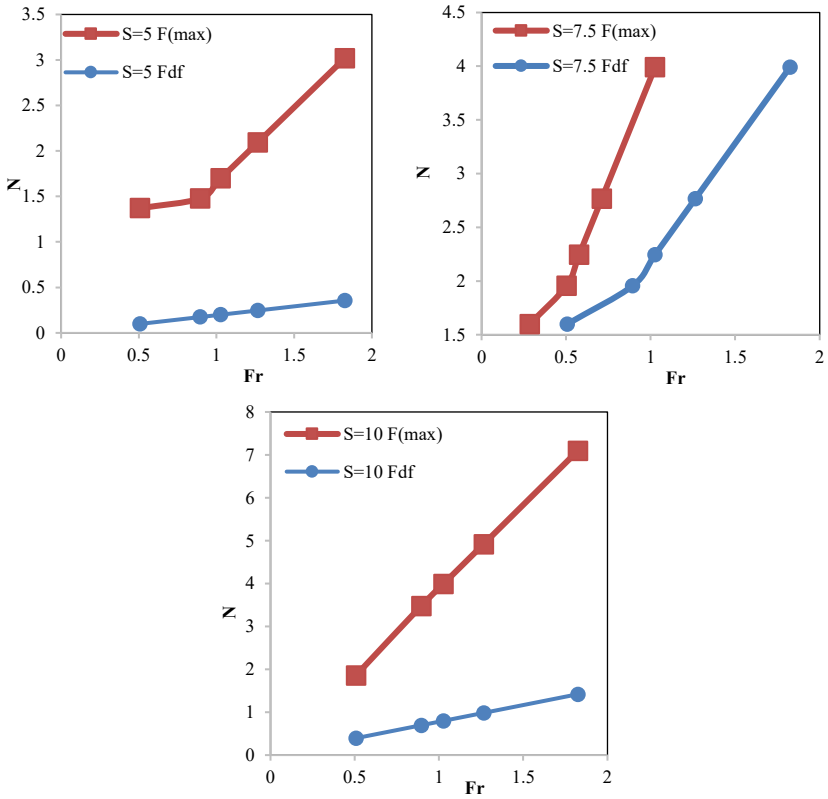


Figure 7. Effect of Froude number on drag force in circular structure

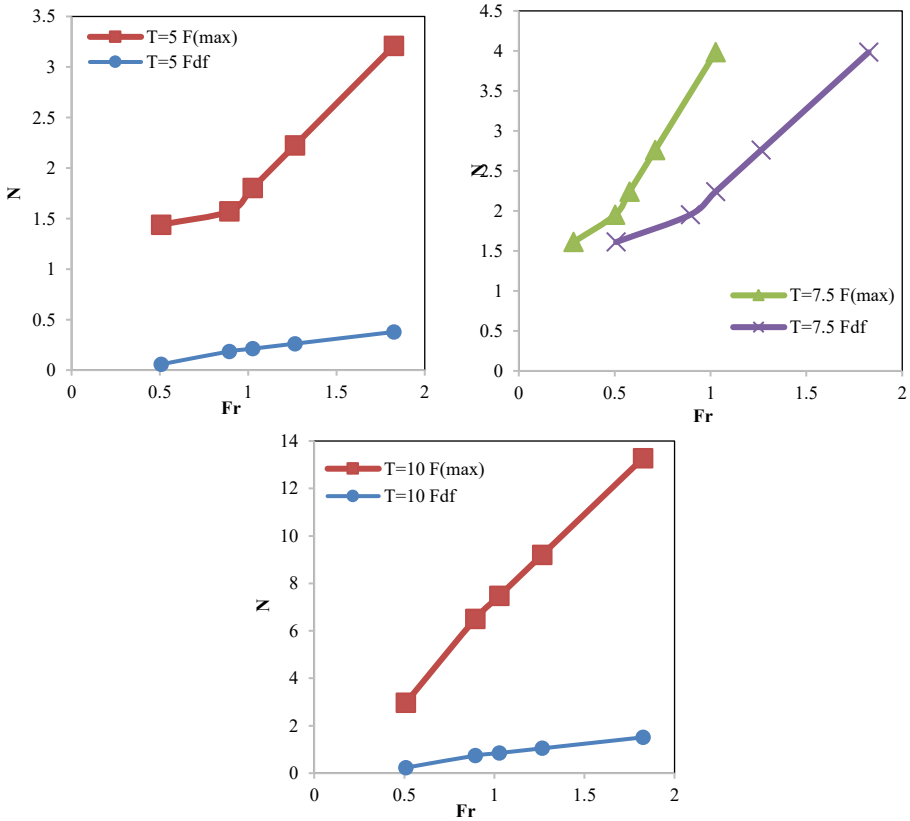


Figure 8. Effect of Froude number on drag force in triangular structure

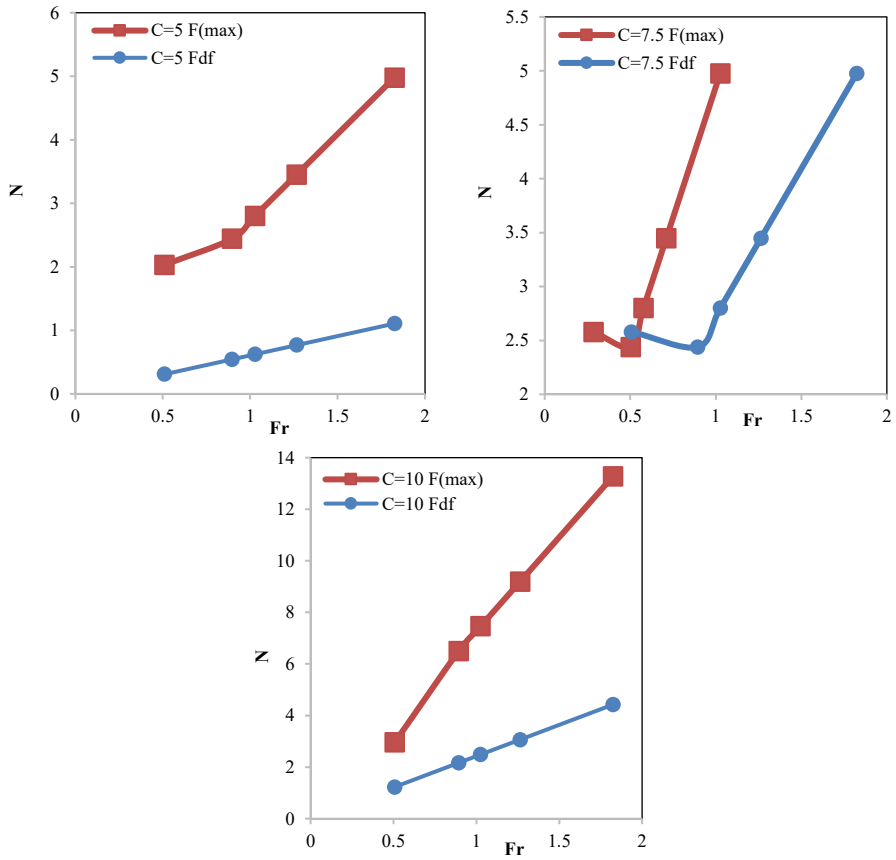


Figure 9. Effect of Froude number on drag force in square structure

Based on Figure 8, with a 50% rise in the dimensions of the structure, the drag force grows by about 230%. Also, the difference between the measured force and the force calculated from Equation 1 is positive in all cases and under some conditions reaches up to 780%.

According to Figure 9, with a 50% increase in the dimensions of the structure, the drag force is enhanced by about 250%.

From the above graphs, it can be concluded that the equation for calculating the applied force has a high calculation error, such that this error reaches up to 780%. This discrepancy between the calculation and reality stems from several main factors. One of them is the error rate in the drag coefficient, which in Equation 1 has a high impact on the amount of force applied. To calculate this number, researchers usually employ Table 1 or a wind tunnel for this number, which in itself causes errors in the calculations of the drag force in the river. The second factor in the calculation error is lack of considering hydraulic conditions such as temperature, viscosity, contamination, and eddy currents. The third reason can be the influence of the structure material on the applied force, which is not captured in Equation 1. Thus, in general, it can be stated that to calculate the drag force, it is better to calculate this number under real conditions with regard to up-to-date technologies and calibrate Equation 1 accordingly.

Also, the geometric shape of the structure has a significant impact on the amount of drag force; so that this effect can be up to about 90%.

The higher drag force in the square model can be attributed to the more severe flow separation and the formation of a larger wake area. In contrast, the triangular model, owing to the reduction in flow separation, created lower values of drag force under the same conditions.

6. Conclusion

The findings indicated that the empirical equations for calculating drag force may differ significantly from direct measurements depending on the base geometry and flow conditions. Future studies are suggested to examine a wider range of geometric shapes, surface roughness, and Reynolds numbers. Also, uncertainty analysis should be performed more thoroughly. Based on the results of this study, it can be stated that:

1. The geometric shape of the structure can affect the drag force by up to 90%.
2. The dimensions of the structure can alter the drag force by up to 250%.
3. Equation 1 (calculated equations) has a significant error in terms of accuracy under the conditions under study.
4. Under some conditions, the difference in the amount of force applied under the same conditions in the calculated method (Equation 1) and the drag force measuring device reaches up to 780%.

Declaration

Conflict of Interest

The authors declare that they have no conflict of interest regarding the publication of this manuscript.

Funding

This research did not receive any specific grant from funding agencies in the public, commercial, or not-for-profit sectors.

Data Availability

The data that support the findings of this study are available from the corresponding author upon reasonable request.

References

1. Tang HJ, Yang RY, Yao HC. Experimental and numerical investigations of a mooring line failure of an aquaculture net cage subjected to currents. Ocean Engineering. 2021 Oct 15;238:109707. 10.1016/j.oceaneng.2021.109707
2. Wang Y, Fu S, Xu Y, Li S, Moan T. Loads on a vessel-shaped fish cage steel structures, nets and connectors considering the effects of diffraction and radiation waves. Marine Structures. 2022 Nov 1;86:103301. 10.1016/j.marstruc.2022.103301.
3. Zhao YP, Liu HF, Bi CW, Cui Y, Guan CT. Numerical study on the flow field inside and around a semi-submersible aquaculture platform. Applied Ocean Research. 2021 Oct 1;115:102824. 10.1016/j.apor.2021.102824.
4. Bi CW, Ma C, Zhao YP, Xin LX. Physical model experimental study on the motion responses of a multi-module aquaculture platform. Ocean Engineering. 2021 Nov 1;239:109862. 10.1016/j.oceaneng.2021.109862.
5. Altaf A, Omar AA, Asrar W. Review of passive drag reduction techniques for bluff road vehicles. IIUM Engineering Journal. 2014 May 31;15(1). 10.31436/iiumej.v15i1.477.
6. Cifuentes C, Kim MH. Numerical simulation of fish nets in currents using a Morison force model. Ocean Syst. Eng. 2017 Jan;7(2):143-55. 10.12989/ose.2017.7.2.143.
7. Anzani HS, Kantoush SA. Effect of Froude number and spacing ratio on drag force and drag coefficient over engineered roughness elements. Case Studies in Thermal Engineering. 2026 May 18:108167. 10.1016/j.csite.2026.108167.
8. Anzani HS, Khalili AM, Kantoush SA, Hamidi M. Hydraulic performance of an isolated strip roughness with varying heights on flow dynamics in open channels. Hydrology Research. 2025 Aug 1;56(8):655-71. 10.2166/nh.2025.167.
9. Chu YI, Wang CM, Zhang H. A frequency domain approach for analyzing motion responses of integrated offshore fish cage and wind turbine under wind and wave actions. Aquacultural Engineering. 2022 May 1;97:102241. 10.1016/j.aquaeng.2022.102241.
10. Bi CW, Zhao YP, Dong GH. Experimental study on the effects of farmed fish on the hydrodynamic characteristics of the net cage. Aquaculture. 2020 Jul 15;524:735239. 10.1016/j.aquaculture.2020.735239.
11. Zhao H, Hu Y, Bi C, Li X. Numerical study on hydrodynamic behaviors of and flow field around UHMWPE plane nets.

Aquacultural Engineering. 2024 Aug 1;106:102397. 10.1016/j.aquaeng.2024.102397.

12. Do TA, Nguyen TH. Assessment of fluid forces on flooded bridge superstructures using the SPH method. Civil Engineering Journal. 2024 Dec 1;10(12):4104-16. 10.28991/CEJ-2024-010-12-019.
13. Han Y, Chen H, Cai CS, Xu G, Shen L, Hu P. Numerical analysis on the difference of drag force coefficients of bridge deck sections between the global force and pressure distribution methods. Journal of Wind Engineering and Industrial Aerodynamics. 2016 Dec 1;159:65-79. 10.1016/j.jweia.2016.10.004.
14. Novak G, Domínguez Alonso, J. M. 3D simulations of flow past a cylindrical bridge pier for determination of drag coefficient as a function of Froude number. Acta Hydrotechnica. 2025, 38(68), 29–37. DOI: 10.15292/acta.hydro.2025.03.
15. Mostefaoui O, Gómez S, Lopez D, Mignot E, Rivière N. Experimental study of the drag force applied by supercritical flows on emerging obstacles. European Journal of Mechanics B/Fluids. 2025, 113, 204262. DOI: 10.1016/j.euromechflu.2025.204262.
16. Okamoto T, Sanjou M. Experimental study on accumulation and failure of driftwood jam and increase in drag force on bridge pier. Journal of Japan Society of Civil Engineers. 2025, 81(16). DOI: 10.2208/jscejj.24-16168.
17. Tang Z, Stoesser T, Huang L. Drag and Lift Forces on Bed Sediments in Open-Channel Flow Through Boulders at Various Froude Numbers. Journal of Geophysical Research: Earth Surface. 2025, 130(8). DOI: 10.1029/2024JF008069.
18. Jianguo W, Haoyu Z, Kai W. Numerical investigation of hydrodynamic forces on twin cylindrical piers with open-channel flow. Journal of Railway Science and Technology. 2026. DOI: 10.1016/j.jrst.2026.06.004.
19. Anzani H S, Kantoush S A. Effect of Froude number and spacing ratio on drag force and drag coefficient over engineered roughness elements. Case Studies in Thermal Engineering. 2026, 83, 108167. DOI: 10.1016/j.csite.2026.108167.
20. Buccolieri R, Sandberg M, Wigö H, Di Sabatino S. The drag force distribution within regular arrays of cubes and its relation to cross ventilation–Theoretical and experimental analyses. Journal of Wind Engineering and Industrial Aerodynamics. 2019 Jun 1;189:91-103. 10.1016/j.jweia.2019.03.022.
21. Buccolieri R, Sandberg M, Wigö H, Di Sabatino S. The drag force distribution within regular arrays of cubes and its relation to cross ventilation–Theoretical and experimental analyses. Journal of Wind Engineering and Industrial Aerodynamics. 2019 Jun 1;189:91-103. 10.1016/j.jweia.2019.03.022.

© 2027 by the authors. Licensee SCU, Ahvaz, Iran. This article is an open access article distributed under the terms and conditions of the Creative Commons Attribution 4.0 International (CC BY 4.0 license) (http://creativecommons.org/licenses/by/4.0/).